LAND SURFACE TEMPERATURE

VISIBLE/INFRARED IMAGER/RADIOMETER SUITE ALGORITHM THEORETICAL BASIS DOCUMENT

Version 5: March 2002

Richard J. Sikorski
Peter S. Kealy

William Emery, Science Team Member
University of Colorado

RAYTHEON SYSTEMS COMPANY
Information Technology and Scientific Services
4400 Forbes Boulevard
Lanham, MD 20706

EDR: LAND SURFACE TEMPERATURE
Doc No: Y2399

Version: 5

Revision: 2

	Function	Name	Signature	Date
Prepared by	EDR Developer	R. SIKORSKI		1/18/02
Approved by	Reviewer	P. KEALY		1/31/02
Approved by	Surface Temperature IPT Lead	R. SIKORSKI		2/11/02
Approved by	Chief Scientist	S. MILLER		2/15/02
Released by	Algorithm IPT Lead	P. KEALY		2/15/02

TABLE OF CONTENTS

<u>Page</u>

LIST OF FIGURES

LIST OF TABLES

<u>Page</u>

SBRS Document #: Y2399

GLOSSARY OF ACRONYMS

ATBD	Algorithm Theoretical Basis Document
ATSR	Along Track Scanning Radiometer
AVHRR	Advanced Very High Resolution Radiometer
ECMWF	European Center for Medium-Range Weather Forecast
FIFE	First International Field Experiment
EDR	Environmental Data Record
IGBP	International Geosphere Biosphere Program
IPO	Integrated Program Office
IR	Infrared
ISLSCP	International Satellite Land Surface Climatology Project
LST	Land Surface Temperature
LUT	Look Up Table
LWIR	Longwave Infrared
MODIS	Moderate Resolution Imaging Spectroradiometer
MODTRAN	Moderate Resolution Atmospheric Radiance and Transmittance Model
MOSART	Moderate Spectral Atmosphere Radiance and Transmittance
MTF	Modulation Transfer Function
MWIR	Midwave Infrared
NCEP	National Centers for Environment Prediction
NPOESS	National Polar-orbiting Operational Environmental Satellite System
P^3I	Pre-Planned Product Improvement
PW	Precipitable Water
SBRS	Santa Barbara Remote Sensing
SDR	Sensor Data Record
SSM/I	Special Sensor Microwave Imager
SST	Sea Surface Temperature
TIR	Thermal Infrared
TOA	Top of Atmosphere
VIIRS	Visible/Infrared Imager/Radiometer Suite

ABSTRACT

This is the Algorithm Theoretical Basis Document (ATBD) for the National Polar-orbiting Operational Environmental Satellite System (NPOESS) Visible/Infrared Imager/ Radiometer Suite (VIIRS) Land Surface Temperature (LST) algorithm for retrieval of the IST Environmental Data Record (EDR). LST is an input variable for other VIIRS products such as soil moisture, land type classification, and infrared (IR) band emissivity.

The VIIRS LST algorithms are based on physical regression methods to retrieve skin LST. They use radiances sensed by VIIRS Infrared (IR) channels. The VIIRS baseline LST algorithm establishes one equation for each land cover type and uses four thermal band brightness temperatures. This algorithm does not need emissivity information.

The atmospheric correction, the complexity of land surface types, and the sensor performance limit the accuracy of satellite LST measurements. The VIIRS LST algorithm requires 2.5 K measurement accuracy and 0.5 K measurement precision. The VIIRS baseline dual split window algorithm (Land cover approach) meets the threshold for all Precipitable Water (PW) ranges and for all viewing angles.

The validation of LST is limited by the availability of *in situ* observations. The VIIRS LST is defined as the skin temperatures of the uppermost layer of the land surface, while *in situ* observations are usually shelter temperatures. Reliable observed or analyzed skin temperatures will be a critical factor in validating the VIIRS LST retrieval.

Raytheon

1.0   INTRODUCTION

1.1 PURPOSE

This document describes the theoretical basis and development process of the LST algorithms, for retrieval of the LST Environmental Data Record (EDR).

1.2 SCOPE

LST is an input variable for other VIIRS products, such as soil moisture. The LST algorithms described in this document will be used to routinely retrieve LST from VIIRS measurements.

The next section of this document provides an overview of the LST retrieval algorithm. A description of the algorithms and their development is presented in Section 3. Section 3 also addresses error budgets, algorithm sensitivity, and validation. Constraints, assumptions, and limitations are identified in Section 4, and Section 5 presents references cited in the document.

1.3 VIIRS DOCUMENTS

This document contains references to other Raytheon VIIRS documents, which are given in italicized brackets:

[SS154640-001] VIIRS System Specification

[PS154640-101] VIIRS Sensor Specification

[Y2386] VIIRS Sea Surface Temperature ATBD

[Y2469] VIIRS Context Level Software Architecture document

[Y2471] - VIIRS Aerosol Module Level Software Architecture

[Y2479] - VIIRS Build SDR Module Level Software Architecture

[Y2502] - Land Surface Temperature Unit Level Detailed Design

[Y2473] VIIRS Surface Temperature Module Level Software Architecture document

[Y3261] - VIIRS Radiometric Calibration ATBD

[Y3277] - VIIRS Aerosol Module Level Interface Control Document

[Y10880] – VIIRS Surface Temperature IP Unit Level Detailed Design Document

1.4 REVISIONS

This is the fifth version of this document, dated March 2002. Substantial contributions to prior versions of this document were made by Donglian Sun, Yimin Ji, Philip E. Ardanuy, and Wenli Yang

2.0   EXPERIMENT OVERVIEW

2.1   OBJECTIVES OF LAND SURFACE TEMPERATURE RETRIEVALS

Land surface temperatures play an important role in land-surface processes on a regional as well as on a global scale. They are of fundamental importance to the net radiation budget at the Earth's surface and to monitoring the state of crops. LST is a good indicator of both the greenhouse effect and the energy flux between the atmosphere and the ground (Mannstein, 1987; Sellers *et al*., 1988). Satellite-derived LST can be assimilated to climate, mesoscale and land surface models to estimate the sensible heat flux and latent heat flux from the Earth's surface. Satellite-based LST measurement has not been used operationally in regional weather forecasting and climate prediction due to large uncertainties. However they have the potential to provide LST information over vast remote regions such as deserts.

The accuracy of satellite LST measurement is primarily limited by the complexity of land surface types, the atmospheric correction, and sensor performance. The published satellite multichannel LST algorithm permit global LST retrievals within 3 to 4 K measurement accuracy. (Becker and Li, 1990; Dozier and Wan, 1994; Li and Becker, 1993).

The overall scientific objective of the VIIRS LST retrieval is to provide improved measurements of global and regional LST fields. The VIIRS LST EDR requires a 2.5 K measurement accuracy and 0.5 K measurement precision. These requirements exceed the published state-of-the-art results. The requirement of measurement precision is difficult to meet because of the large variations of LST in both space and time. LSTs can vary by 10 K in just a few meters and by 50 K over the daily cycle (Prata, 1993). However, the VIIRS dual split window algorithm (Land cover approach) meets the requirements, because this method overcomes surface emissivity effects.

2.2   INSTRUMENT CHARACTERISTICS

The VIIRS sensor has been designed based on the NPOESS sensor requirements derived from EDR system specifications. VIIRS bands in the Longwave Infrared (LWIR) region have been placed to optimize their use for Sea Surface Temperature (SST) determination. Bands in the LWIR are usually located near the maximum Earth radiance. The influence of ozone and other atmospheric absorbers should be avoided. Figure 1 shows Moderate Resolution Atmospheric Radiance and Transmittance Model (MODTRAN) simulated radiances at satellite altitude for thermal infrared spectra. There are a total of five standard atmospheres shown. There are two wavelength regions suitable for LWIR band selection: 8–9 μm and 10–13 μm. VIIRS LWIR bands are located in the two spectral regions. Figure 2 shows the MODTRAN simulated atmospheric transmittance for five standard atmospheres. It shows that the 8–9 μm and 10–13 μm regions are transparent to the atmosphere. The details of LST band selection can be found in Caselles *et al*., 1997, however VIIRS bands were optimized for SST.
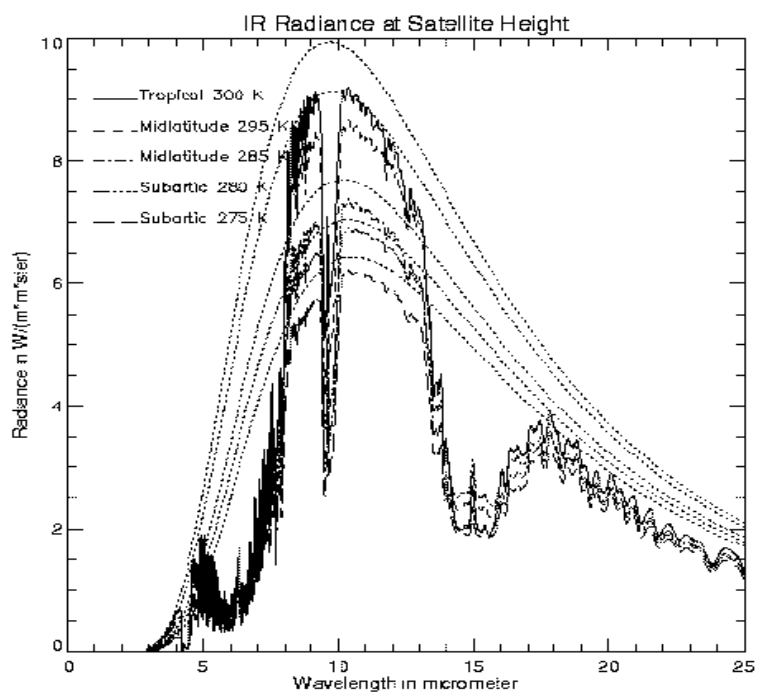
Figure 1. IR radiance at the satellite for five atmospheres simulated by MODTRAN. The dashed lines are calculated from the Planck function.
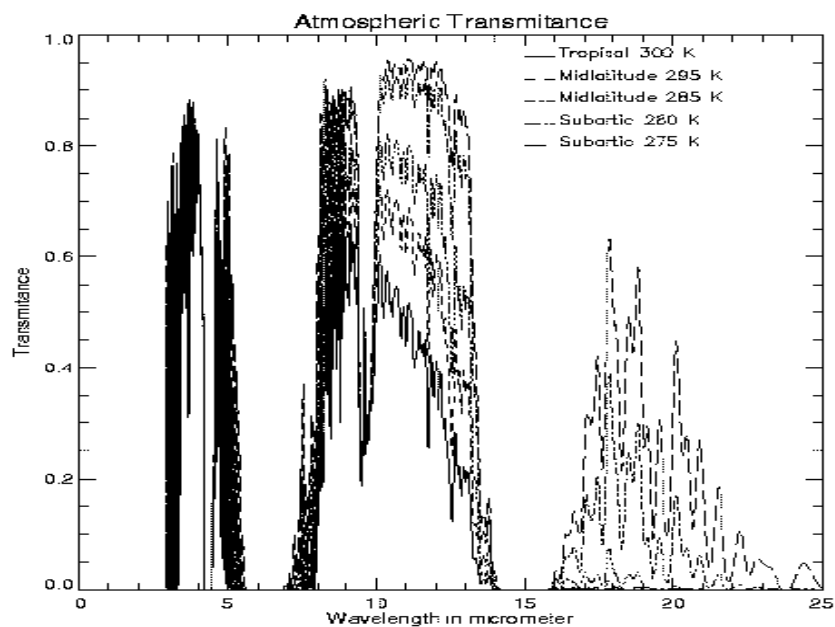
Figure 2. Atmospheric transmittances for five atmospheres. The dashed lines are calculated from the Planck function.

2.3   LAND SURFACE TEMPERATURE RETRIEVAL STRATEGIES

If we were to solve the LST problem physically, we would have to know the atmospheric profile for each pixel (unlikely to be available operationally in the near future), and also the surface emissivity for each band. Because the surface emissivity for each band is different, the number of unknowns is always larger than the number of equations. A number of ways have been suggested to physically retrieve the surface temperature and emissivity. These methods include the two temperature method (Watson, 1992), the temperature emissivity separation method (Kealy and Hook, 1993), and the day/night method (Wan and Dozier, 1996). However, these methods demand many more LWIR bands than in the VIIRS baseline design

VIIRS testbed results have shown that Land Cover regression methods, with a separate set of coefficients for each land cover type, are able to meet requirements by compensating for variations in emissivity among surface types, while employing the type of atmospheric correction used in SST retrievals.

Land Cover Approach Regression methods

1A. Four band Algorithm (Baseline Solution):

VIIRS dual split window day/night LST algorithm establishes one equation for each surface type by using 4 VIIRS bands (10.8, 12, 3.75, and 4.005 μm), with added solar zenith angle correction during the daytime:

Daytime:

$$LST_i = a_0(i) + a_1(i)T_{11} + a_2(T_{11} - T_{12}) + a_3(i)(\sec\theta - 1) + a_4(i)T_{3.75} + a_5(i)T_{4.0} + a_6(i)T_{3.75}\cos\varphi$$
$$+ a_7(i)T_{4.0}\cos\varphi + a_9(i)(T_{11} - T_{12})^2 \qquad i = 1, \ 23 \tag{1}$$

Nighttime:

$$LST_i = b_0(i) + b_1(i)T_{11} + b_2(T_{11} - T_{12}) + b_3(i)(\sec\theta - 1) + b_4(i)T_{3.75} + b_5(i)T_{4.0} + b_6(i)T_{3.75}^2$$
$$+ b_7(i)T_{4.0}^2 + b_9(i)(T_{11} - T_{12})^2 \qquad i = 1, \ 23 \tag{2}$$

Where i is the index of 23 VIIRS testbed surface types. Note that the operational LST algorithm will use the VIIRS Surface Type EDR which delivers the 17 International Geosphere Biosphere Program (IGBP) surface types.

1B. Two band Algorithm (Fallback Solution):

For each of the VIIRS testbed 23 surface types, establish one equation by using 11 and 12 μm split window.

$$LST_i = a_0(i) \quad + a_1(i)\,T_{11} + a_2(i)\,(T_{11} - T_{12}) + a_3(i)\,(\sec\theta - 1) + a_4(i)\,(T_{11} - T_{12})^2 \qquad i = 1, 23 \tag{3}$$

3.0   ALGORITHM DESCRIPTION

The VIIRS cloud cover mask, snow/ice mask, and land/ocean mask are used to eliminate cloud-contaminated pixels, ice-covered pixels, and ocean pixels. Land cover type is retrieved from visible and near-IR bands by the VIIRS Land software module. The LST is retrieved using a regression equation, with separate coefficients for each land cover type. In the VIIRS baseline dual split window algorithm, only land type is needed.

3.1   PROCESSING OUTLINE

The coefficients for the regression equations will be obtained using MODTRAN and a global database through our simulation processes. Figure 3 depicts the processing concept for LST retrievals. In the VIIRS baseline dual split window algorithm, one equation is developed for each land type. There are a total of 23 equations for the global data in the VIIRS testbed. The VIIRS Land Cover EDR will deliver the 17 IGBP land cover types for operational use. (Figure 3).
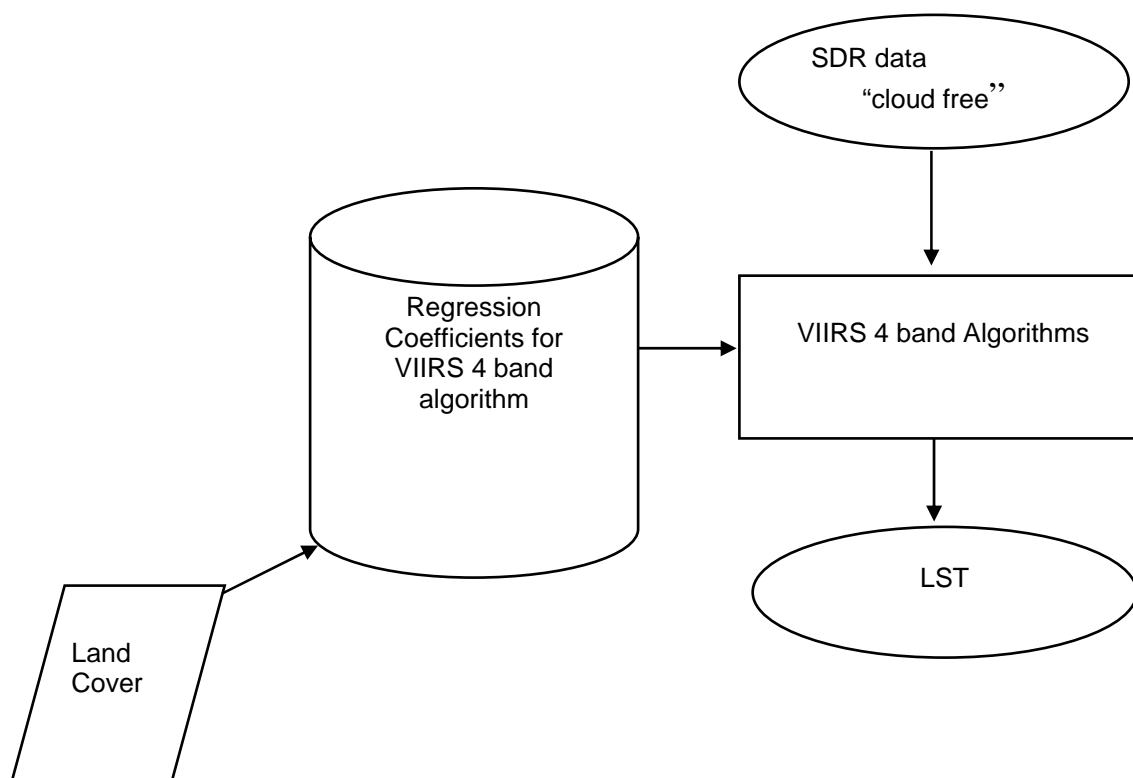

Figure 3. LST flowchart: Land cover approach - One equation for each land surface type.

3.2   ALGORITHM INPUT

3.2.1   VIIRS Data

VIIRS inputs required for the LST algorithm are Land Cover classification, IR radiances, cloud mask, ice/snow mask, and land/ocean mask.

3.2.2   Non-VIIRS Data

The operational VIIRS LST algorithms do not require non-VIIRS data.

3.3   THEORETICAL DESCRIPTION OF LAND SURFACE TEMPERATURE RETRIEVAL

3.3.1   Physics of the Problem

In clear sky conditions, the outgoing infrared spectral radiance at the top of atmosphere can be represented by:

$$L(\lambda,\mu) = \tau(\lambda,\mu)\varepsilon(\lambda,\mu)B(\lambda,T_s) + L_a(\lambda,\mu) + L_s(\lambda,\mu,\mu_0,\varphi_0)$$
$$+ L_d(\lambda,\mu,\mu_0,\varphi_0) + L_r(\lambda,\mu,\mu_0,\varphi_0)$$

(4)

Where τ is the transmissivity, ε the surface spectral emissivity, B the Plank function, L_a the thermal path radiance, L_s the path radiance resulting from scattering of solar radiation. L_d is the solar radiance and L_r the solar diffuse radiation and atmospheric thermal radiation reflected by the surface. λ is the wavelength. $\mu = \cos(\theta)$, $\mu_o = \cos(\psi)$, where θ is the satellite zenith angle, ψ the solar zenith angle. φ_o is the azimuth angle.

The wavelength is the wavelength center of a narrow interval because there is no way to measure the exact monochromatic signal as a continuous function of wavelength by satellite sensors. Equation 4 can be used in the 3–14 *μm* range. It requires complete calculations of the atmospheric radiative transfer to determine the values of all terms on the right side. This equation has been used in many atmospheric radiation models including LOWTRAN (Kneizys *et al*., 1988), MODTRAN (Berk *et al*., 1987), and Moderate Spectral Atmospheric Radiance and Transmittance (MOSART) (Cornette *et al*., 1994).

For LWIR bands, L_d, L_s, and L_r are negligible. Therefore, only the first two terms on the right side of the above equation are important. The first term represents the surface contribution term, and it is the gray-body radiance emitted by the earth's surface. The second term is the atmospheric contribution term, and is the vertically integrated effect of emission from every atmospheric layer modulated by the transmittance of the air above that emitting layer.

$$L(\lambda,\mu) = \varepsilon_0(\lambda,\mu)B(\lambda,T_s)\tau_0(\lambda,\mu) + \int_{\tau_0}^{1} B(\lambda,T_p)d\tau(\lambda,\mu,\rho)$$

(5)

Where τ_0 is the transmittance at the Earth's surface.

In order to infer the surface information, we should choose window channels with small atmospheric contributions. As shown in Figure 1, the wavelength between 3.5–4.2 µm, 8–9 µm, and 10–13 µm are some typical atmospheric windows, with less atmospheric absorption. For a perfect window, the total atmospheric transmittance $\tau_0(\lambda\ \mu)$ should be 1.0, and the transmittance weighting function should be 0. But as we see from Figure 2, the transmittances at these windows are not 1.0. This is mainly the result of the water vapor absorption.

In order to see the water vapor's contribution at the atmospheric window channel, we did some simulations to the 2415 profiles offered by the IPO over land surfaces under clear sky conditions by using MODTRAN 3.7. The following five window bands are simulated: 3.75 µm, 10.8 µm (AVHRR channel 4), 12 µm (AVHRR channel 5), and two new VIIRS bands, including 4.005 µm and 8.55 µm.

As we can see from the transmittance vs. surface skin temperature distribution, shown as Figure 4a, at warmer temperatures (285–310 K), for 10.8 and 12 µm channels and the 8.55 µm channel, the transmittances decrease significantly. Most values are below 0.8. This is why most existing split window algorithms using the 11 and 12 µm channels get larger errors in the temperature range 285–310 K. The transmittance for the Midwave Infrared (MWIR) channel 3.75 µm and 4.005 µm is more stable, with less change to the surface skin temperature; most values are above 0.8. From this aspect, MWIR 3.75 µm and 4.005 µm channels are better window channels than the LWIR 11, 12, and 8.55 µm channels. The most stable channel is at 4.005 µm. From the transmittance vs. PW (Figure 4b), we can also see that the transmittance at the 4.005 µm channel is the most stable. It changes very little with the column water vapor amount. While the transmittance at 3.75 µm channel has a linear relationship with the precipitable water, the transmittances at 11, 12, and 8.55 µm decrease significantly as the water vapor increases and the relationship is also not linear. The information from MWIR window channel can be used when we retrieve warmer surface temperatures.

From the difference between the surface temperature and brightness temperature vs. precipitable water distribution, as shown in Figure 4c, the temperature deficit (Ts-Tb) at IR window channels 11, 12, and 8.55 µm is very stable, while the surface temperature at MWIR channels 3.75 and 4.005 µm can be much lower than the brightness temperature, sometimes by more than 10 degrees. This is because in the daytime, the MWIR channel contains both reflected solar radiation and radiation emitted by the surface and the atmosphere, this is the so-called solar glint. So the best way to retrieve surface temperature is to appropriately combine LWIR and MWIR window channels.
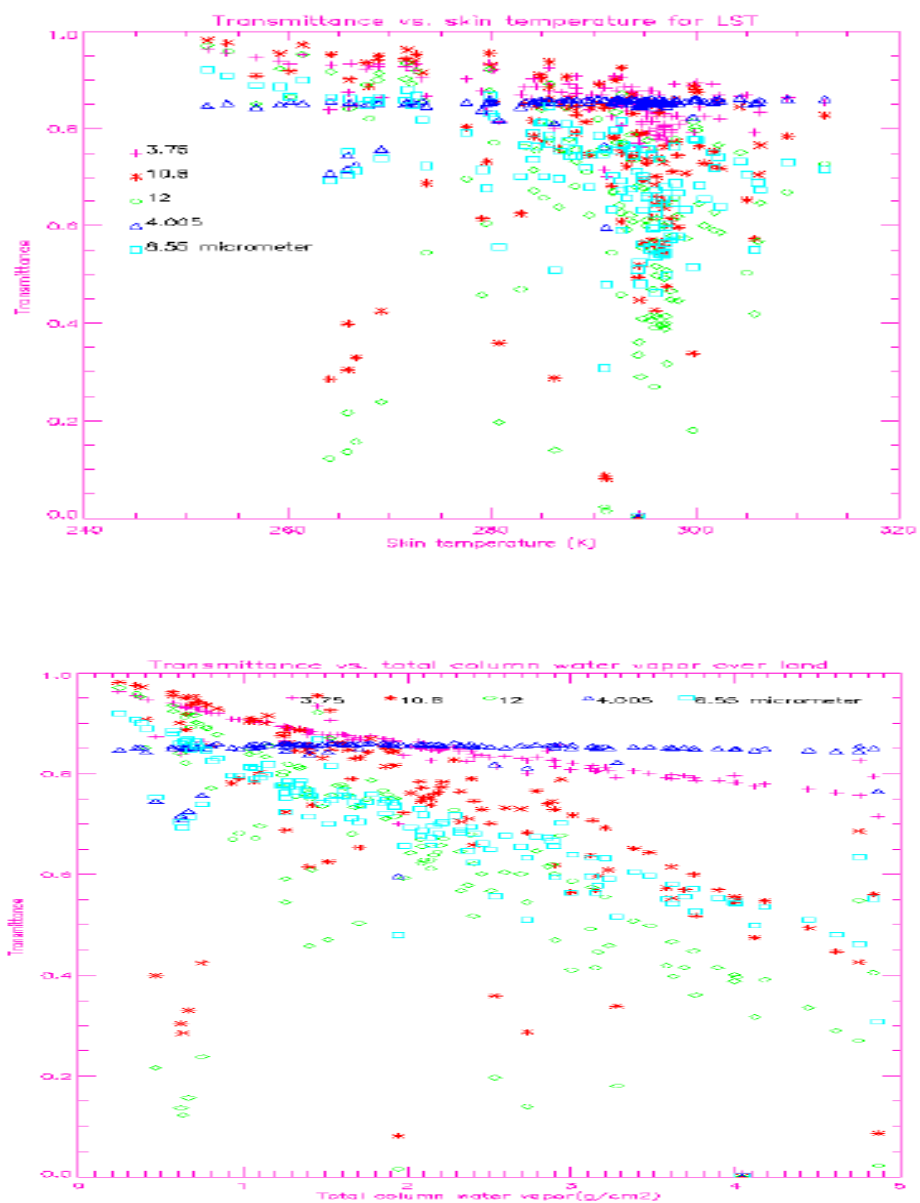
Figure 4a. Upper Panel: Transmittance vs. LST. 4b. Lower Panel: Transmittance vs. PW over land.

Raytheon
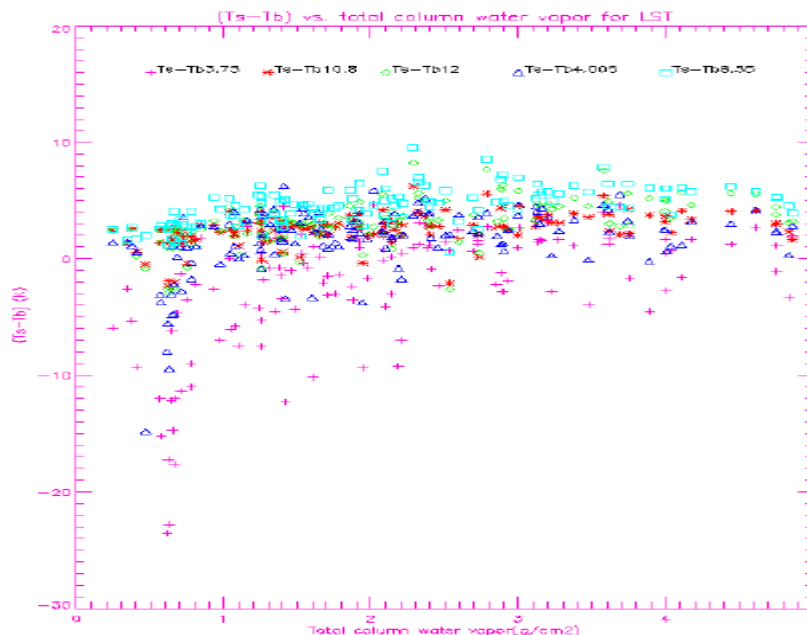
Figure 4c. Temperature deficits (T$_s$-T$_b$) vs. PW distribution.

Currently, most existing LST algorithms are variants based on Becker and Li's split window technique (1990).

$$Ts = (A1 + A2\frac{1-\varepsilon}{\varepsilon} + A3\frac{\Delta\varepsilon}{\varepsilon^2})\frac{T_{11}+T_{12}}{2} + (B1 + B2\frac{1-\varepsilon}{\varepsilon^2} + B3\frac{\Delta\varepsilon}{\varepsilon^2})(T_{11}-T_{12}) + C \qquad (6)$$

Where $\varepsilon = (\varepsilon_{11} + \varepsilon_{12})/2$ and $\Delta\varepsilon = \varepsilon_{11} - \varepsilon_{12}$. ε_{11} and ε_{12} are the emissivities at 10.8 μm and 12 μm bands respectively. T_{11} and T_{12} are the brightness temperatures at 10.8 μm and 12 μm bands respectively.

One of the major difficulties in the development of the LST algorithm is the considerable spectral variation in emissivities for different land surface types. Observation of emissivity spectra shows that in general, emissivity spectra with high values exhibit little variation, while those with lower values exhibit a greater variation, such as grass, as shown in Figure 5.

Emissivity distribution with band
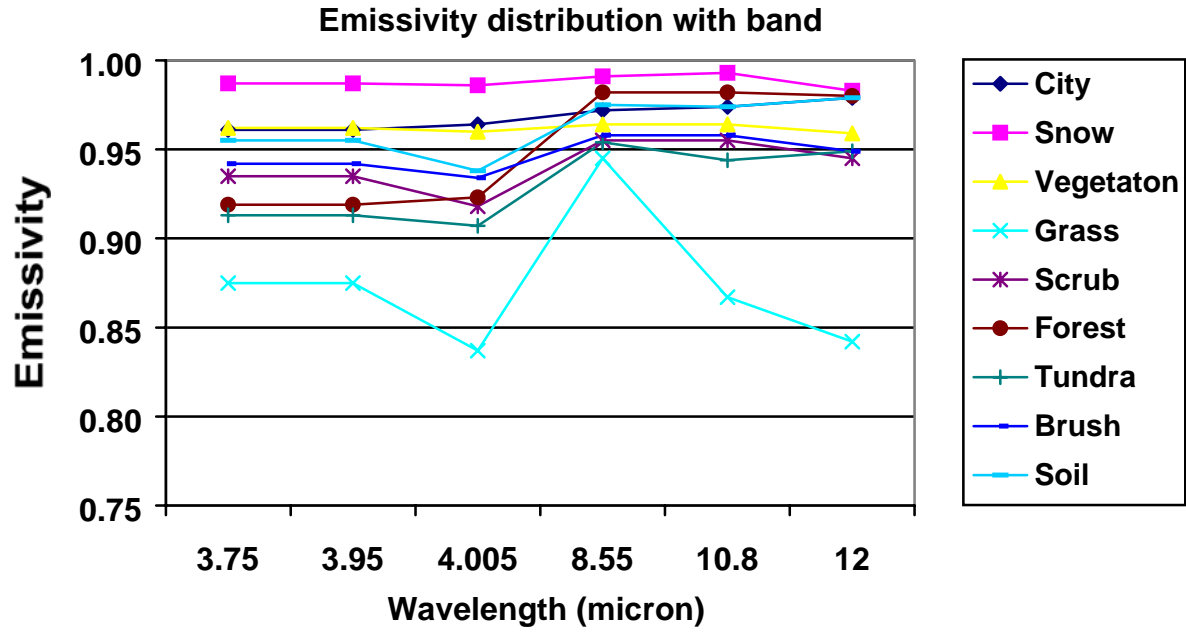
Figure 5. Variation in emissivity for different surface types.

If we ignore the change of emissivity for a certain land surface type, the radiance error introduced by the atmosphere ΔL can be represented by:

$$\Delta L = B(\lambda, T_s) - L(\lambda, \mu) = B(\lambda, T_s) - \tau(\lambda, \mu)B(\lambda, T_s) - L_a(\lambda, \mu)$$

$$= - \int_1^{\tau(\lambda,\mu)} B(\lambda, T_s)d\tau(\lambda, \mu, p) + \int_1^{\tau(\lambda,\mu)} B(\lambda, T_p)d\tau(\lambda, \mu, p) \quad (7)$$

$$= - \int_1^{\tau(\lambda,\mu)} (B(\lambda, T_s) - B(\lambda, T_p))d\tau(\lambda, \mu, p)$$

From the Planck function we find:

$$\Delta L = \frac{\partial B}{\partial T}\Delta T = \frac{\partial B}{\partial T}(T_s - T_\lambda) \quad (8)$$

For an optically thin gas the following approximations can be made:

$$d\tau = d\{\exp(-k_\lambda L)\} = -k_\lambda dl \quad (9)$$

where k_λ is the absorption coefficient and l is the optical path-length.

If we assume that the Planck function is adequately represented by a first order Taylor series expansion in each channel window, then:

$$B(\lambda, T_s) - B(\lambda, T_p) = \left.\frac{\partial B(\lambda, T_p)}{\partial T}\right|_{T_s} (T_p - T_s) \tag{10}$$

Substituting Equations 8, 9, 10 into Equation 7, we obtain:

$$T_s - T_\lambda = k_\lambda \int_1^\tau (T_s - T_p) dl \tag{11}$$

Therefore, if we select two spectral regions of the atmosphere, we will have two linear equations with different k_λ to solve simultaneously.

For example if we consider the two channels as $\lambda=1$ and $\lambda=2$, then we get:

$$T_s - T_1 = -(T_2 - T_1) k_1 / (k_2 - k_1) \tag{12}$$

This equation is similar to the SST equation, but can only be used for one land type, assuming the band emissivity does not vary within this land type. Figure 6a shows the relationship between band temperature deficits T_s-T_{11} and T_s-T_{12} for forests. The data are global data with 17,885 skin temperatures and atmospheric profiles. The relationship is rather linear, which confirms that for a particular land type, the linear split window algorithm used in SST retrieval can be adopted for LST. Figure 6b is similar to Figure 6a, but for simulations of 23 land cover types. There is much more variation in this figure; the relationship is not linear. Emissivities, therefore, have to be considered as an important factor for Becker and Li's 1990 LST algorithm.

For land surfaces, the emissivity for each channel changes with surface type. Table 1 shows the band-averaged emissivities for the 23 VIIRS testbed surface types derived from MOSART spectra. The VIIRS testbed surface types contain a majority of the IGBP land surface types. The VIIRS LAND EDR will deliver the 17 IGBP land surface types for operational LST retrieval. The differences between 10.8 µm and 12 µm bands are small for most of the types, thus making the use of separate sets of coefficients for each land type in the VIIRS baseline land cover approach feasible.
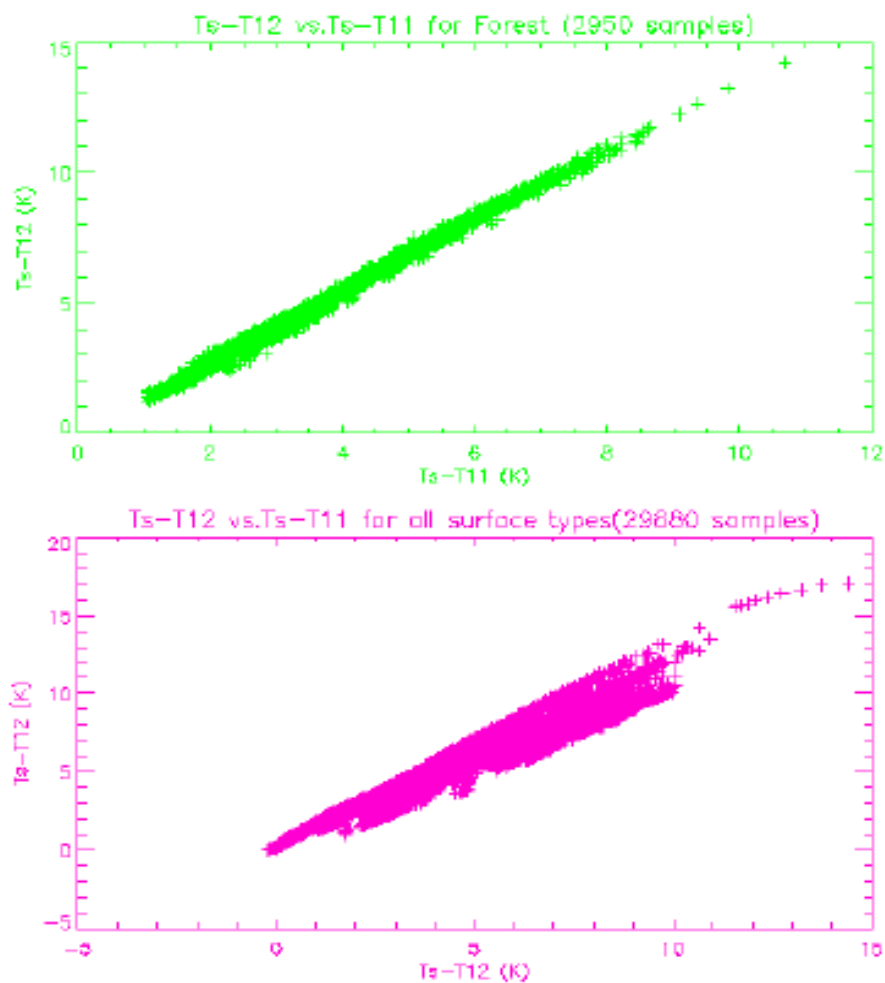
Figure 6. (a) Relationship between temperature deficits of 10.8 µm and 12 µm bands for forest only. (b) Relationship between temperature deficits of 10.8 µm and 12 µm bands for all 23 land types.

Table 1. Band-Averaged Emissivities of 23 Surface Types in VIIRS testbed Bands 10, 11, 12, SST1, SST2, SST4.

Surface Type Index	Type of Materials	$\varepsilon_{3.75}$	$\varepsilon_{10.8}$	ε_{12}	$\varepsilon_{3.99}$	$\varepsilon_{4.00}$	$\varepsilon_{8.55}$
1	Water	0.980	0.990	0.990	0.980	0.980	0.985
2	Old snow	0.987	0.993	0.983	0.987	0.986	0.991
3	Sea ice	0.987	0.995	0.983	0.987	0.982	0.992
4	Compacted soil	0.930	0.957	0.967	0.930	0.895	0.965
5	Tilled soil	0.951	0.970	0.977	0.951	0.926	0.975
6	Sand	0.500	0.950	0.980	0.500	0.550	0.900
7	Rock	0.800	0.915	0.960	0.800	0.840	0.895
8	Cropland	0.962	0.964	0.959	0.962	0.960	0.964
9	Meadow grass	0.875	0.867	0.842	0.875	0.837	0.945
10	Scrub	0.935	0.955	0.945	0.935	0.918	0.955
11	Broadleaf forest	0.952	0.962	0.956	0.952	0.957	0.962
12	Pine forest	0.905	0.990	0.990	0.905	0.907	0.990
13	Tundra	0.913	0.944	0.949	0.913	0.907	0.954
14	Grass-soil	0.908	0.921	0.918	0.908	0.872	0.957
15	Broadleaf-pine forest	0.919	0.982	0.980	0.919	0.923	0.982
16	Grass-scrub	0.905	0.911	0.893	0.905	0.877	0.950
17	Soil-grass-scrub	0.915	0.929	0.923	0.915	0.885	0.956
18	City	0.961	0.974	0.979	0.961	0.964	0.972
19	Pine-brush	0.920	0.973	0.967	0.920	0.913	0.973
20	Broadleaf-brush	0.942	0.958	0.949	0.942	0.934	0.958
21	Wet soil	0.955	0.974	0.979	0.955	0.938	0.975
22	Scrub-soil	0.932	0.956	0.959	0.932	0.904	0.961
23	Broadleaf (70%)—Pine (30%)	0.938	0.970	0.966	0.938	0.942	0.970

Figure 7 shows the emissivity change as a function of surface types for four VIIRS MWIR and LWIR bands. LWIR band emissivities are relatively stable for all land types. The changes of MWIR emissivity are larger at land type 6 (sand) and type 7 (rock).

Channel emissivity vs. Land type
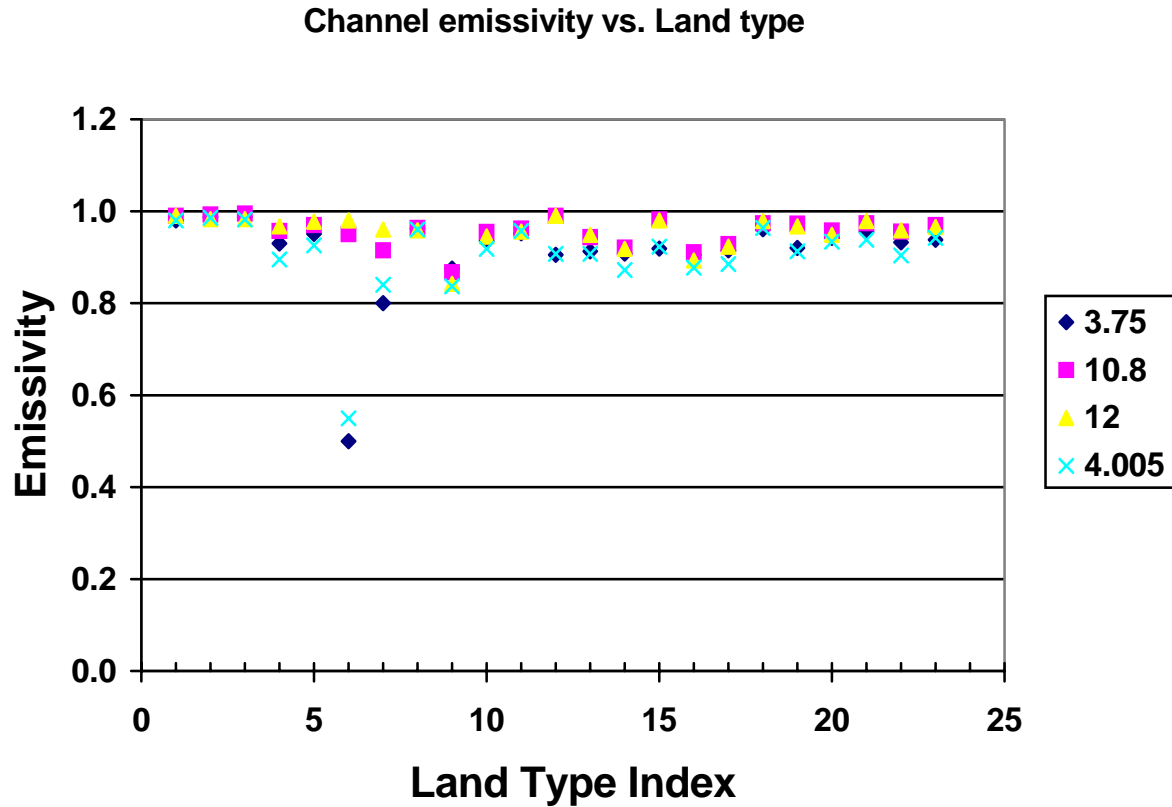
Figure 7. Channel emissivities for 23 land types.

In general, Equation 11 can be written as:

$$T_s = CT_b$$

The coefficient vector C, relating observed brightness temperatures to LST, is determined using a regression method by solving:

$$C = YX^T(XX^T)^{-1} \tag{13}$$

The Y matrix contains a large number of training LSTs and the X matrix contains brightness temperatures from VIIRS LWIR and MWIR channels. In general, the X matrix may include non-linear terms.

Currently, the LST uncertainty from the regression algorithm is about 1 ~ 3 K.

3.3.2 Mathematical Description of the Algorithm

Based on the previous section's discussion of the physics of the problem, the mathematical descriptions of the algorithm can be simply stated.

Baseline Algorithm:

VIIRS dual split window day/night LST algorithm establishes one equation to each surface type by using 4 VIIRS bands (10.8, 12, 3.75, and 4.005 μm), and it added a solar zenith angle correction during the daytime:

Daytime:

$$LST_i = a_0(i) + a_1(i)T_{11} + a_2(T_{11} - T_{12}) + a_3(i)(\sec\theta - 1) + a_4(i)T_{3.75} + a_5(i)T_{4.0} + a_6(i)T_{3.75}\cos\varphi$$
$$+ a_7(i)T_{4.0}\cos\varphi + a_9(i)(T_{11} - T_{12})^2 \qquad i = 1,\ 23 \tag{14}$$

Nighttime or day and night:

$$LST_i = b_0(i) + b_1(i)T_{11} + b_2(T_{11} - T_{12}) + b_3(i)(\sec\theta - 1) + b_4(i)T_{3.75} + b_5(i)T_{4.0} + b_6(i)T_{3.75}{}^2$$
$$+ b_7(i)T_{4.0}{}^2 + b_9(i)(T_{11} - T_{12})^2 \qquad i = 1,\ 23 \tag{15}$$

Where i is the index of 23 VIIRS testbed surface types. Note that the operational LST algorithm will use the VIIRS Surface Type EDR which delivers the 17 International Geosphere Biosphere Program (IGBP) surface types.

Backup Algorithm:

1A. Two band Algorithm (Fallback Solution):

For each of the 23 VIIRS testbed surface types, establish one equation by using 11 and 12 μm split window.

$$LST_i = a_0(i)\quad + a_1(i)\,T_{11} + a_2(i)\,(T_{11} - T_{12}) + a_3(i)\,(\sec\theta - 1) + a_4(i)\,(T_{11} - T_{12})^2 \qquad i = 1,\ 23 \tag{16}$$

3.3.3 Test Data Set Description

The Test Data Sets we used to develop the VIIRS LST algorithms are described in earlier versions of this document. Simulations presented here used National Center for Environmental Prediction (NCEP) global snapshot surface temperature data set with matching atmospheric profiles at the resolution 2.5 x 2.5 degrees;

NCEP global snapshot surface temperature data set

The global snapshot surface temperature data set is at 2.5^{o} by 2.5^{o} resolution supplied by the National Centers for Environment Prediction (NCEP), with matching atmospheric profiles.

3.3.4   Variance and Uncertainty Estimates

There are mainly three geophysical factors that contribute to the uncertainty of satellite LST retrieval: land surface classification, emissivity determination errors and atmospheric correction errors. In addition sensor errors need to be accounted for.

Land cover approach

For a specific surface type, the deficits between the surface temperature and the brightness temperature at 11 μm and 12 μm have very good linear relationship, therefore split window algorithms can be adopted to a specific surface type. Land Cover Maps exist and will be improved during the MODIS era, Figure 8. For each surface type, we establish one set of regression coefficients between the surface temperature and 11μm and 12 μm brightness temperature. Figure 9a displays the LST precision for different land surface types. The lines present the results from the VIIRS fallback split window algorithm for various land surface types (Land cover approach). This figure shows that the Land Cover method can improve the retrieval precision for all surface types. Figure 9b shows the summary statistics of retrieval for all the surface types vs. different sensor noise model. The sensor noise level specification is equivalent to noise model 3.

Figure 10 shows the utility of a solar zenith correction function being added to the equation during daytime retrievals, using the VIIRS baseline dual split window algorithm (Land cover approach). The solar zenith correction is particularly useful at higher temperatures. Figure 11 and Figure 12 show the estimated performances of the baseline algorithm as a function of viewing angle and temperature for both day and night respectively.
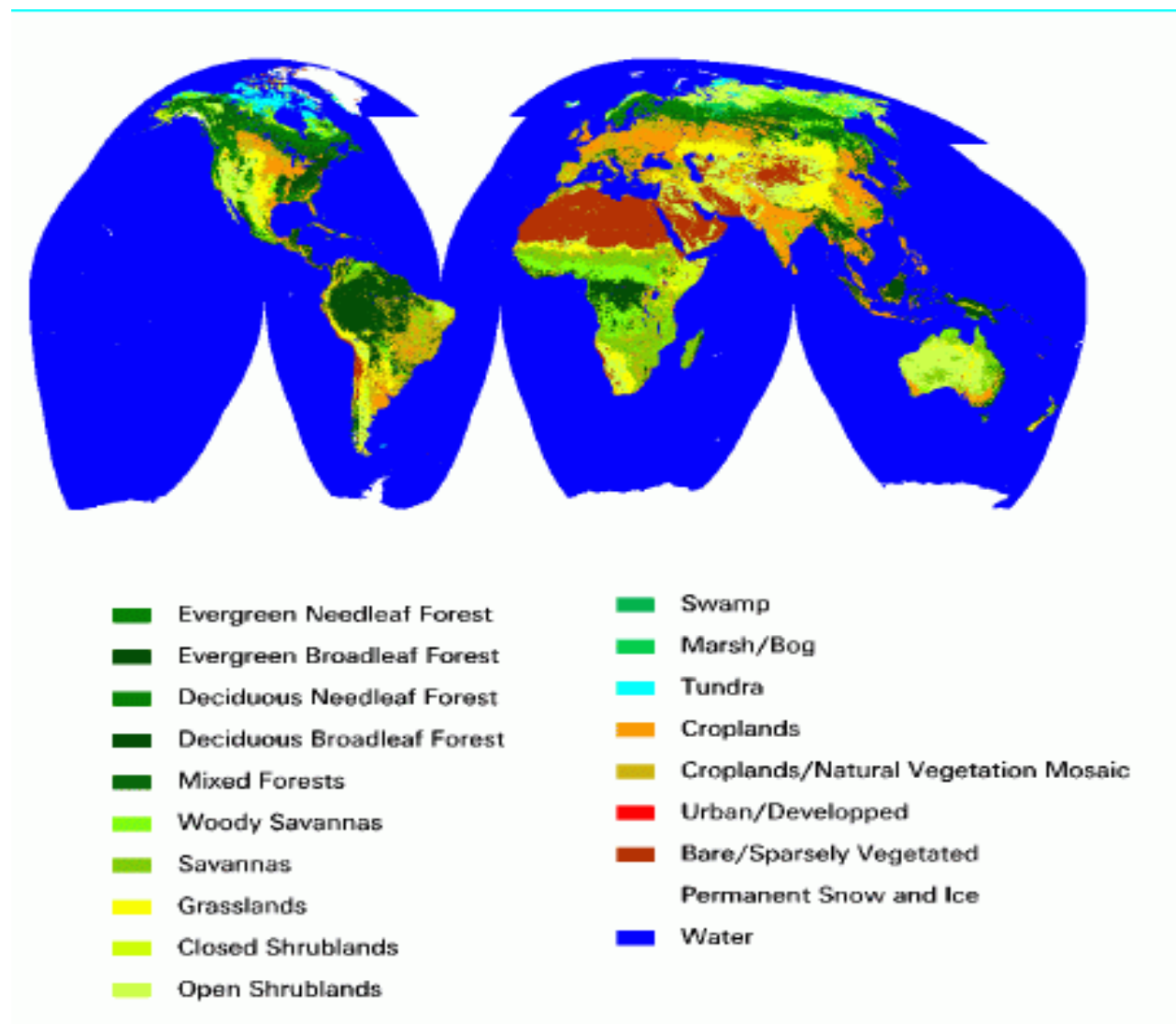
Figure 8. Global land cover distribution at 8km resolution in July 1992.

LST Precision (Split Window)
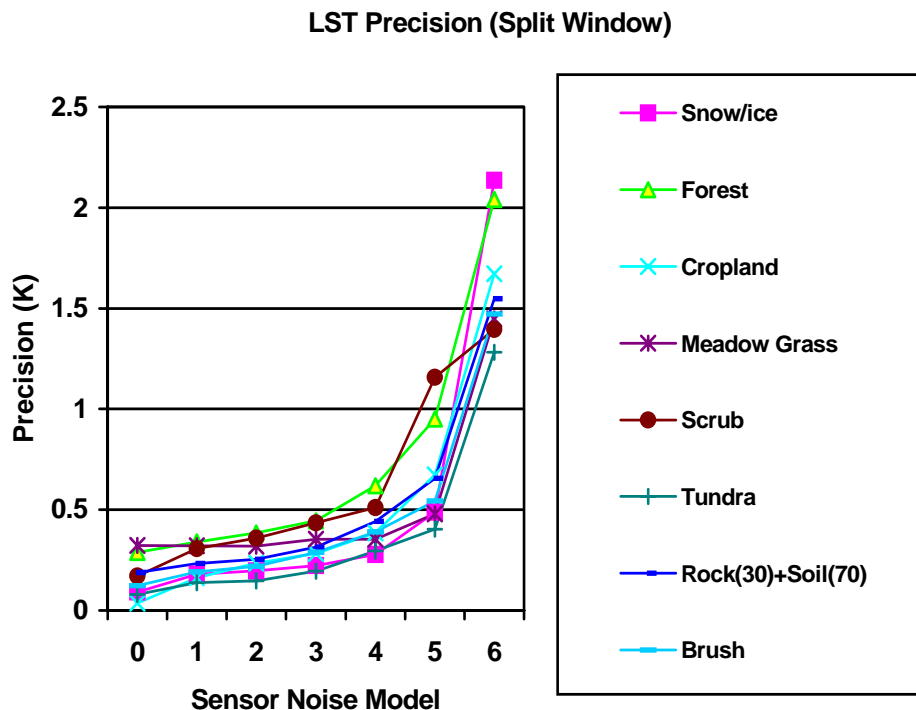
Figure 9a. Precision analysis for the VIIRS fallback split window (Land cover approach) retrieval method.

LST precision (split window)
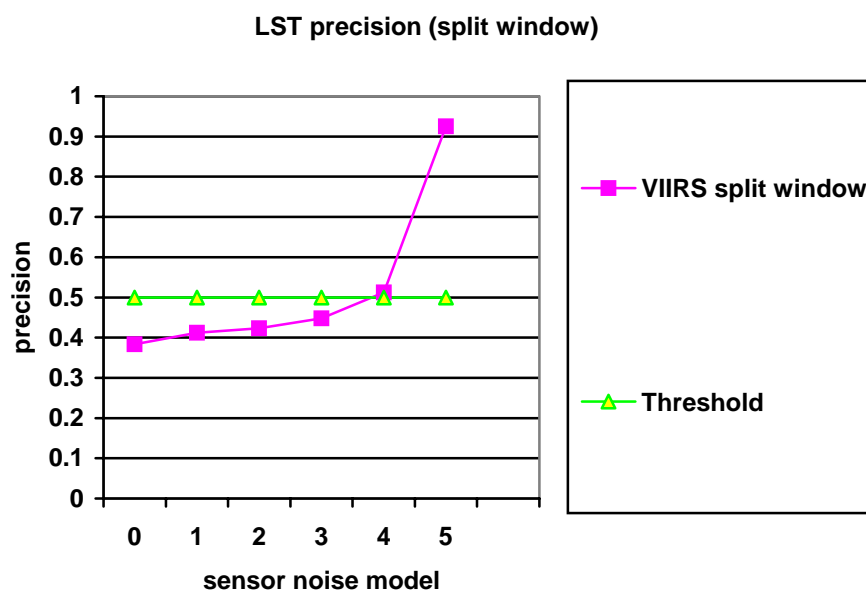
Figure 9b. Global LST retrieval precision for the VIIRS fallback split window (Land cover approach) retrieval method.
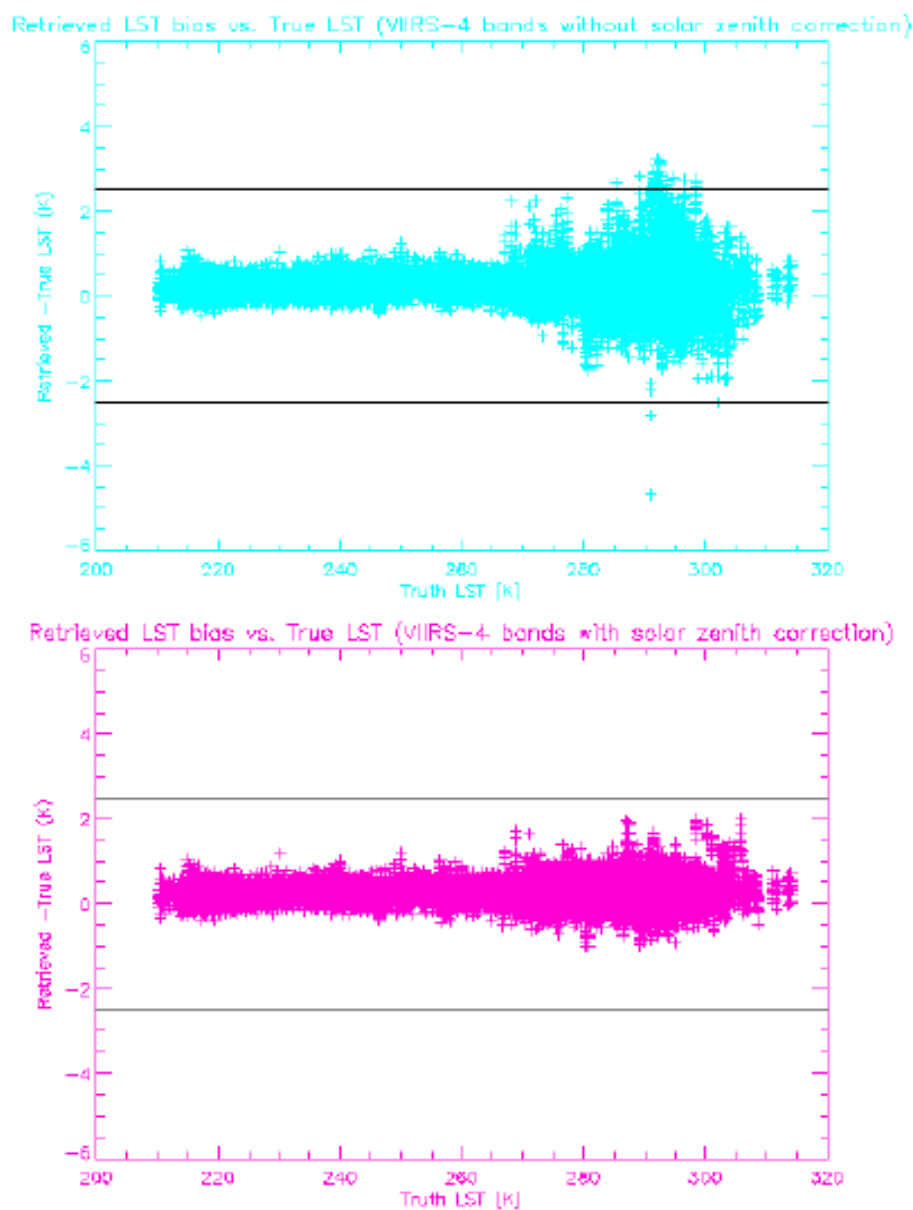
Figure 10. LST retrieval error vs. LST distribution for VIIRS baseline dual split window algorithm (Land cover approach). The upper panel: Without solar zenith angle correction. The bottom panel: With solar zenith angle correction during the daytime.
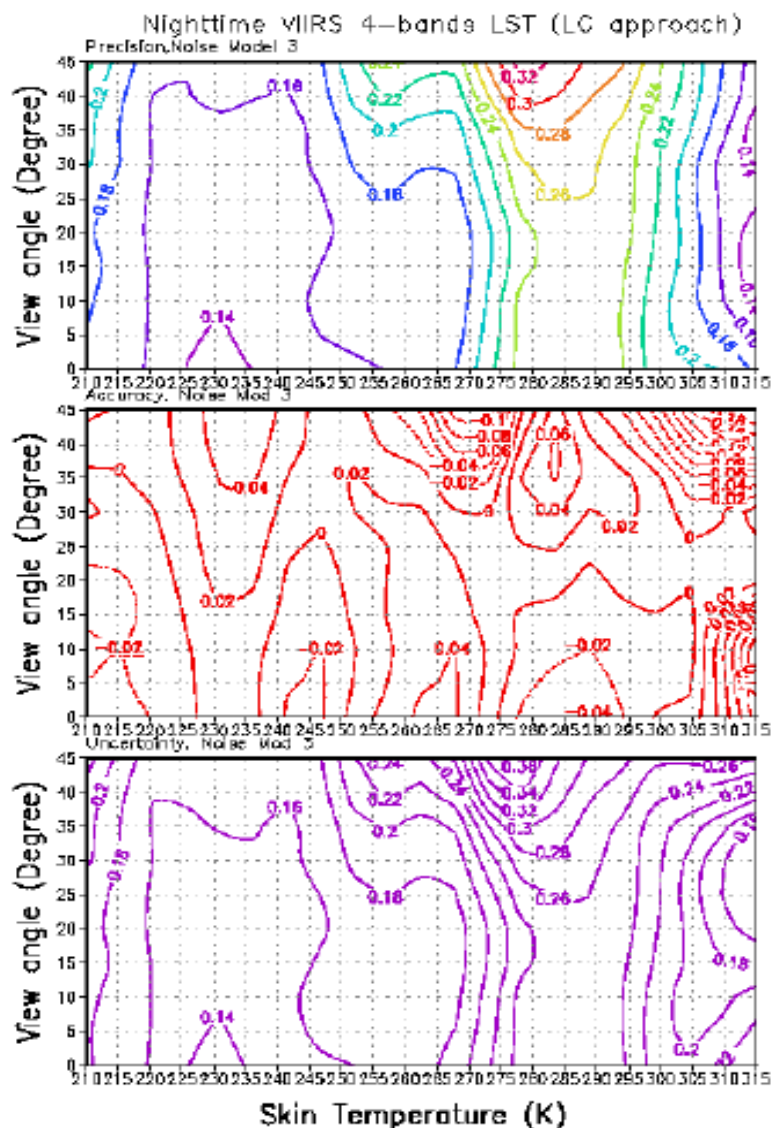
Figure 11. Nighttime LST precision (upper panel), accuracy (middle) and uncertainty (bottom) distribution over satellite viewing angle and LST by using VIIRS baseline dual split window algorithm (Land cover approach).

Figure 12. Daytime LST precision (upper panel), accuracy (middle) and uncertainty (bottom) distribution over satellite viewing angle and LST by using VIIRS baseline dual split window algorithm (Land cover approach) with solar zenith correction.
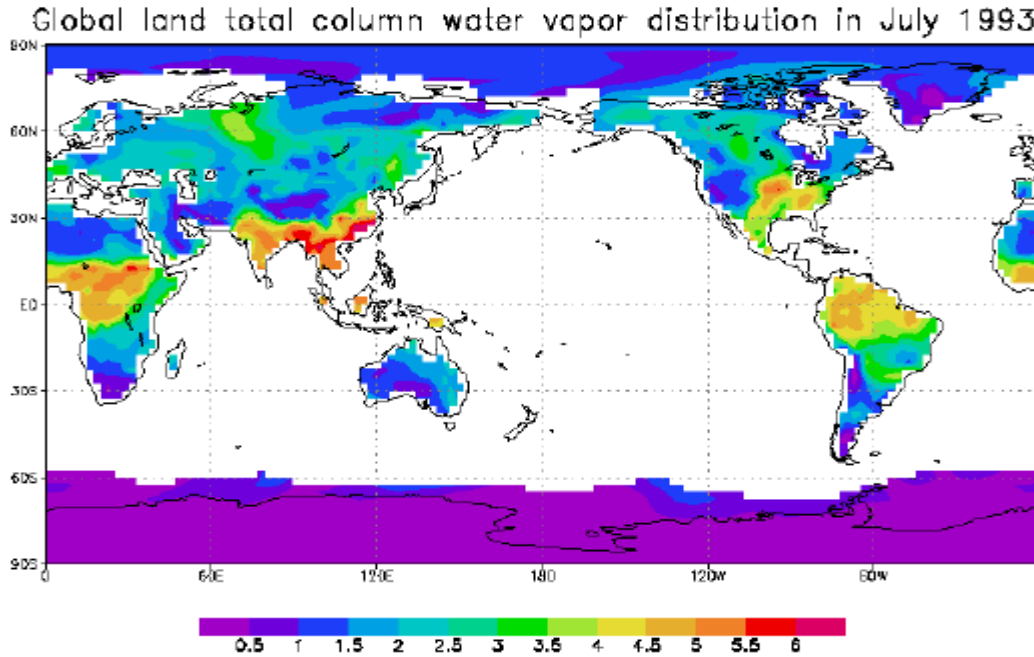
Figure 13. PW distribution over land in our global dataset.

Water vapor's effect

In window channels, the main atmospheric effect comes from the water vapor absorption. So the PW amount has important effect to LST retrieval error. Figure 13 show the PW distribution in this global dataset.

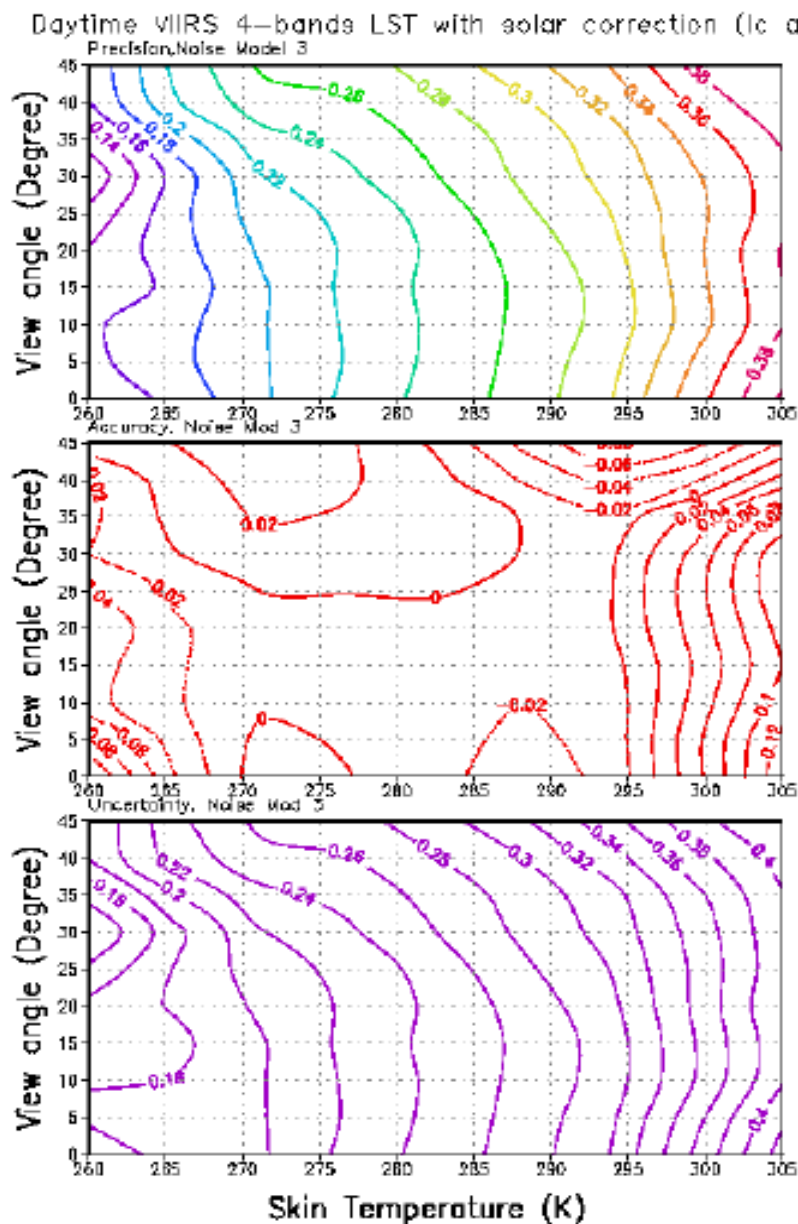There is higher PW at higher temperature, as shown in Figure 14, and larger LST errors at warmer temperature above 280 K. We analyzed the relationship of LST retrieval error at temperature range 280-305 K with water vapor amount.

LST precision is worse at PW 0.5-1.0 g/cm^2. These retrievals correspond to rock, sand, desert or sea ice areas. Harris and Mason (1992) revealed that for a given change in surface temperature ΔT_0, the resulting changes in brightness temperatures in the two LWIR wavebands has the following relationship:

$$\frac{\Delta T_2}{\Delta T_1} = \frac{\varepsilon_2}{\varepsilon_1} \frac{\tau_2(0, p_0)}{\tau_1(0, p_0)}$$

$$\tau_\lambda(0, p_0) = exp(-k_{w\lambda} U_w(0, p_0)) exp(-k_{o\lambda} U_o(0, p_0))$$

So surface emissivities changes, as well as atmospheric transmittance changes, cause brightness temperatures to change. If we divide the absorbing gases into water vapor and other gases:

$$\frac{\Delta T_2}{\Delta T_1} = \frac{\varepsilon_2}{\varepsilon_1} exp((k_{w1} - k_{w2}) U_w(0, p_0)) exp((k_{o1} - k_{o2}) U_o(0, p_0))$$

where $k_{W\lambda}$ and KO_λ are the band–averaged absorption coefficients for water vapor and other gases, respectively; U_w $(0,p_0)$ and U_o $(0,p_0)$ are the total column contents of water vapor and other gases, respectively. Supposing that the magnitude $(k_{w1}-k_{w2})$ U_w $(0,p_0)$ is small, it is reasonable to take the first-order expansion, as U_w $(0,p_0)$ is the total column water or precipitable water W, so we have

$$\frac{\Delta T_2}{\Delta T_1} \approx \frac{\varepsilon_2}{\varepsilon_1}(1 + KW + const.\ )$$

So surface emissivity and atmospheric PW cause the brightness temperature to change and therefore cause LST retrieval error. At PW 0.5-1.0 g/cm^2, the emissivity changes for the 3.75 and 4.005 μm bands over rock, sand, and desert cause LST retrieval error.

The VIIRS baseline dual split window algorithm (Land cover approach) shows LST precision can meet the threshold 0.5 K at all PW range and all viewing angles, shown as Figure 15. This is because this method overcomes the surface emissivity's effect.

Figure 14. Water vapor vs. surface skin temperature distribution.

Figure 15. The LST precision, accuracy and uncertainty distribution with the PW and viewing angle by using the VIIRS baseline dual split window algorithm (Land cover approach).
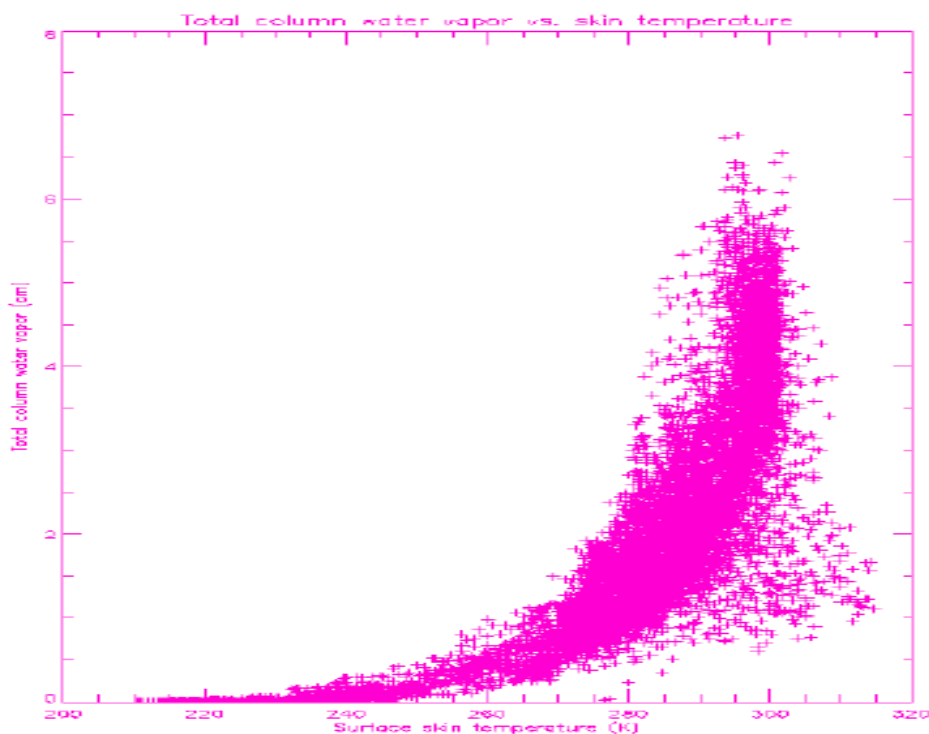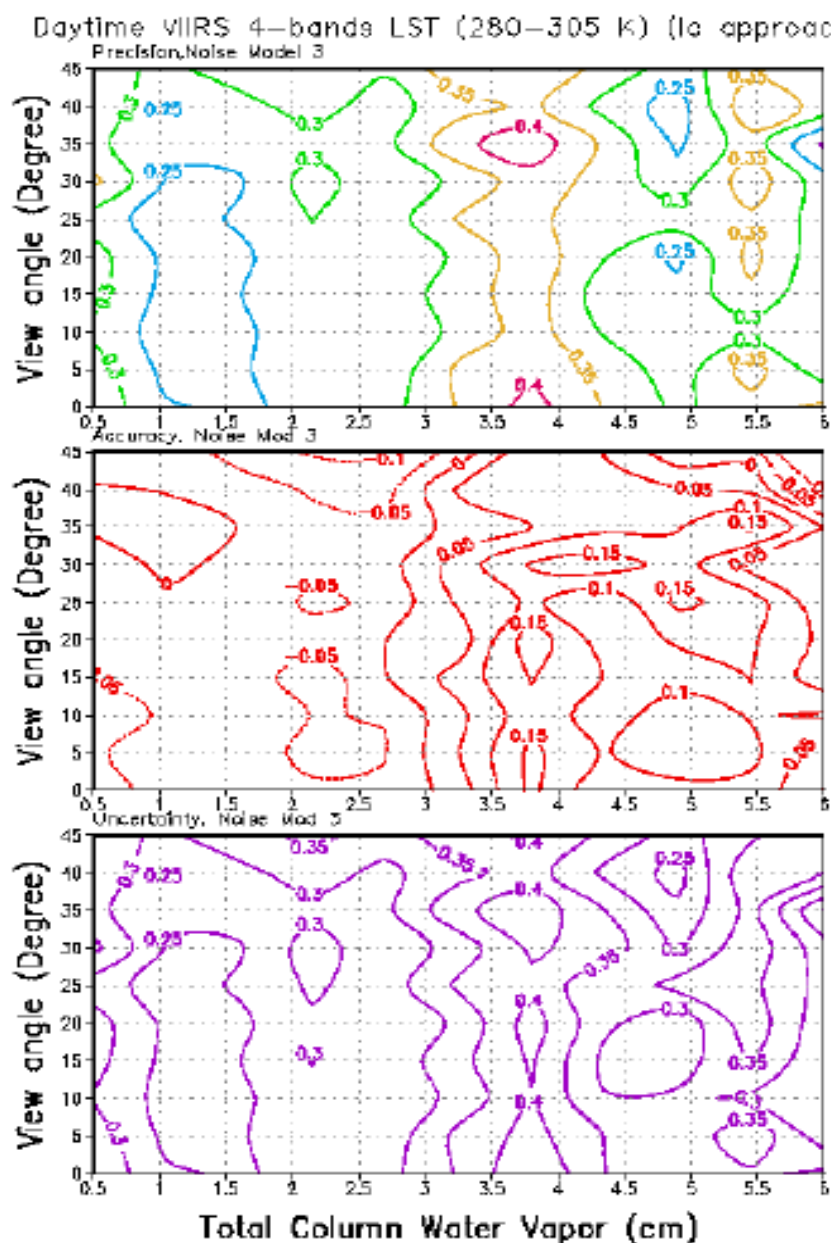
3.3.5 Validation problem

All of the tests above were performed based on simulation data, i.e., the truth LST was assumed to be known. For real-time data, the validation of global LST retrievals from satellite measurements is problematic since satellites measure skin temperature while ground truths provided by the global observational system are shelter temperatures. Although skin LSTs from a few field sites – such as the First International Satellite Land Surface Climatology Project (ISLSCP) Field Experiment (FIFE) – are now available (Prata, 1994; Wan and Snyder, 1996), they are not globally representative. Prata (1994) and many others have addressed the difficulty of obtaining ground truth LST. *In situ* LSTs can be measured with contact thermometers, as well as thermal infrared spectrometers. The contact thermometers measure LST at a point, while the satellites measure the mean LST over a pixel area. The LST may vary significantly within a pixel area, and therefore, a single pixel may require the use of a number of thermometers.

In reality, both spatial and time variability of land surface temperatures is greater than that of sea surface temperature. This makes the validation of LST retrieval from satellite data more difficult than with SST validation. Weng and Grody, (1998) tried to use shelter temperature in the early morning to validate LST retrieval from satellite SSM/I data. They found that the difference between surface skin temperature and shelter temperature is lowest at early morning. This validation, however, is limited to early morning. Another validation problem is the time. The number of *in situ* observations that match the satellite measurement in both time and space will be small: the *in situ* LST was not observed at the exact time when the satellite passed.

3.4 ALGORITHM SENSITIVITY STUDIES

3.4.1 Land Cover

Our baseline algorithm VIIRS dual split window algorithm depends on an accurate knowledge of land surface types. The VIIRS vegetation index EDR accuracy requirement is 70%. But, usually, accuracy above 80% can be achieved by using neural networks or decision tree algorithms. When we did an experiment with a 20% land cover classification error, the LST retrieval process is a little bit worse than the testbed results presented in this document, but the VIIRS baseline dual split window LST algorithm can still meet the threshold of 0.5 K. This is because land cover classifications by using neural networks or decision trees misclassify to a similar surface type that still has similar emissivity characteristics. For instance, broadleaf forests may be misclassifying as pine forests, pine brush as broadleaf brush, or wet soil as scrub soil. Grass, however, cannot be classified as rock or sand. So this is why an algorithm based on surface types may not cause great errors, even with a 20% land cover classification error, see Figure 16.

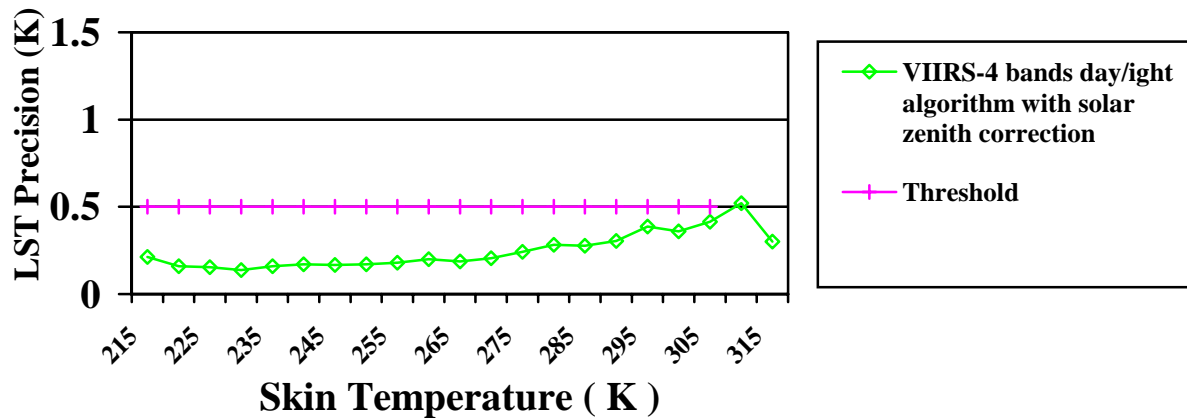**Precision v.s. Temperature and different algorithms for NCEP global data set with sensor noise model 3.**

Figure 16. LST precision vs. temperature by using VIIRS baseline dual split window day/night algorithm with 20% land cover classification error.

3.5 PRACTICAL CONSIDERATIONS

3.5.1 Numerical Computation Consideration

In order to retrieve LST within an operational timeframe, statistical algorithms that meet quality requirements have been developed that are much quicker than physical modeling methods. Pre-generated LUTs are used to speed processing yet retain flexibility.

3.5.2 Programming and Procedural Considerations

The simplicity of all the algorithms described in this document translates into very small amounts of code using basic mathematical routines. Computationally intensive processes are performed offline, with results delivered as re-generated LUTs. VIIRS Phase II efforts are largely software-focused, and the methodology for this development work is based on sound and proven principles, as discussed in the VIIRS Algorithm Software Development Plan *[Y6635]*. The present maturity of the VIIRS software is detailed in the VIIRS Algorithm Software Maturity Assessment document *[Y6661]*. The maturity and remaining Phase II tasks for the algorithms themselves is summarized in the VIIRS Algorithm/Data Processing Technical Report *[Y7040]*. The software designs relevant to the IST Unit are summarized in the VIIRS Context Level Software Architecture *[Y2469]*, Surface Temperature Module Level Software Architecture *[Y2473]*, and Land Surface Temperature Unit Level Detailed Design *[Y2502]*. These designs are tested at the system level as described in the most recent versions of the VIIRS Software Integration and Test Plan *[Y3236]*, Algorithm Verification and Validation Plan *[Y3237]*, and System Verification and Validation Plan *[Y3270]*. A summary of the ultimate strategy for

operational application of the system of VIIRS algorithms is provided in the VIIRS Operations Concept document *[Y2468]*. The VIIRS Interface Control Document (ICD *[Y2470]*) provides more detail on the specifics of ancillary data requirements for Vegetation Index and other VIIRS products.

3.5.3 Configuration of Retrievals

Adjustable parameters for the retrieval of the LST products allow post-launch updating of regression coefficients. The flexibility built into the architecture also allows easy implementation of future P^3I developments.

3.5.4 Quality Assessment and Diagnostics

A number of parameters and indicators are reported in the LST product as retrieval diagnostic flags. Statistical information is reviewed for quality assessment. **Error! Reference source not found.** lists the available quality flags. The final list of delivered flags will be determined in the operational environment.

Table 2. LST Quality Flags

VIIRS LST flags	bits
Land/Water Background	3
Cloud Detection	2
LST quality	2
Spare	1

3.5.4 Exception Handling

Cloud pixels identified by the cloud mask will be skipped. Pixels with bad data will also be skipped and flagged.

3.6 ALGORITHM VALIDATION

3.6.1 Pre-Launch Validation

The atmospheric correction algorithm will be derived pre-launch by radiative transfer modeling to simulate the VIIRS infrared channel measurements. Selected radiosondes from the operational network stations or field campaigns will be used in VIIRS simulations for the development of the atmospheric correction algorithm. Measurements from the portable radiometers and a TIR spectrometer will be used to characterize the surface temperature fields and validate the atmospheric correction algorithms. The assimilated meteorological fields provided by NCEP and ECMWF provide a valuable description of surface temperature over land. These fields will be

used in conjunction with radiative transfer modeling to simulate the VIIRS measurements, validate the radiosonde data, and provide direct input to the radiative transfer modeling process.

Measurements from AVHRR, the Along Track Scanning Radiometer (ATSR), and MODIS will be used in the pre-launch phase to study the error characteristics of the LST retrieval.

3.6.2 Post-Launch Validation

The post-launch validation activities are designed primarily to test the LST retrieval algorithm. Several fundamentally different data sets are needed to provide an adequate sampling of the atmospheric conditions and LST to validate the VIIRS IR radiance and retrieved LST fields. Highly focused field experiments are necessary to understand the atmospheric processes that limit the accuracy of the retrieved LST. Sites will be selected globally to validate VIIRS LST retrieval. (MODIS LST ATBD, version 3.2). Relatively flat areas of highly unmixed surface type will yield the highest quality measurements for validation. Portable radiometers and a TIR spectrometer will be calibrated with the same blackbody radiation source. Long-term global data sets are necessary to provide a monitoring capability that would reveal calibration drift and the consequences of extreme atmospheric events. Validation is required over the lifetime of the NPOESS mission.

4.0   ASSUMPTIONS AND LIMITATIONS

A major limitation of the VIIRS LST retrieval is that it can only be done under clear sky conditions. Ground truth LST measurements are necessary for calibration and validation, but it is difficult to obtain true skin LST over the full range of land surface types. Typically, LST varies significantly on a sub-pixel scale, and over short timescales, so that satellite retrieved LST necessarily represents a pixel-averaged measurement at a snapshot in time.

5.0   REFERENCES

Becker, F. (1987): The impact of spectral emissivity on the measurement of land surface temperature from a satellite. *Int. J. Remote Sens*. 11: 369-394.

Becker, F., and Z. L. Li (1990). Toward a local split window method over land surface. *Int. J. Remote Sens*. 11, 369-393.

Becker, F., and Li, Z. -L. (1995) Surface temperature and emissivity at various scales: definition, measurement and related problems. *Remote Sens. Rev.* 12:225-253.

Berk, A., L. S. Bemstein, and D. C. Robertson (1987). MODTRAN: A moderate resolution model for LOWTRAN. Rep. GLTR-89-0122, Burlington, MA: Spectral Sciences, Inc.

Caselles, V., E. Valor, C. Coll, and E. Rubio (1997). Thermal band selection for the PRISM instrument 1. Analysis of emissivity-temperature separation algorithms. *J. Geophys. Res*., 102, 11145-11164.

Cornette, W. M., P. K. Acharya, D. C. Robertson, and G. P. Anderson (1994). Moderate spectral atmospheric radiance and transmittance code (MOSART). Rep. R-057-94(11-30), La Jolla, CA: Photon Research Associates, Inc.

Crag, R., M. Sugita, and W. Brutsaert, 1995: Satellite-derived surface temperature with boundary layer temperatures and geostrophic winds to estimate surface energy fluxes, J. Geophys. Rev., vol. 100, no. D12, 25447-25451.

Dozier, J., and Z. Wan (1994). Development of practical multiband algorithm for estimating land surface temperature from EOS/MODIS data. *Adv. Space Res*., 13, 81-90.

Harris, A. R., and I. M. Mason (1992). An extension to the split-window technique giving improved atmospheric correction and total water vapor. Vol. 13, no. 5, 881-892.

Jackson, R. D., R. J. Reginato, and S. B. Idso, 1977: Wheat Canopy temperature: a practical tool for evaluating water requirements, *Water Resour. Res*., vol. 13, 651-656.

Kimura, F. and A. P. Shimiru, 1994: Estimation of sensible and latent heat fluxes from soil surface temperature using a linear air land heat transfer model, *J. Appl. Meteorol*. , vol. 33, no. 4, 477-489.

Kealy, P. S., and S. J. Hook (1993). Separating temperature and emissivity in thermal infrared multispectral scanner data: Implications for recovering land surface temperature. *IEEE Trans. Geosci. Remote Sens*., 31, 1155-1164.

Kneizys, F. X., E. P. Shettle, L. W. Abreu, J. H. Chetwynd, G. P. Anderson, W. O. Gallery, J. E. A. Selby, and S. A. Clough (1988). Users guide to LOWTRAN7. Rep. AFGL-TR-88-0177, Bedford, MA: Air Force Geophys. Lab.

Li, Z. L., and F. Becker (1993). Feasibility of land surface temperature and emissivity determination from AVHRR data. *Remote Sens. Environ*, 43, 67-85.

Mannstein, H. (1987). Surface energy budget, surface temperature and thermal inertia in Remote Sensing Applications. In Meteorology and Climatology, ed. R. A. Vaughan and D. Reidel. I, NATO ASI Ser. C: Math. Phys. Sci. Vol 201, pp. 391-410, Dordrecht Netherlands: A Reidel Publishing Co.

Prata, A. J. (1993). Land surface temperature derived from the Advanced Very High Resolution Radiometer and the Along-Track Scanning Radiometer I. Theory. *J. Geophys. Res*., 98, 16689-16702.

Price, J. C. (1984), Land surface temperature measurements form the split window channels of the NOAA-7/AVHRR. J. Geophys. Res. 89: 7231-7237.

Running, S. W., 1991: Computer simulation of regional evapotranspiration by integrating landscape biophysical attributes with satellite data, in Land Surface Evaporation: Measurements and Parameterization, ed. T. J. Schmugge and J. C. Andre, New York: Springer-Verlag.

Running, S. W., C. Justice, V. Salomonson, D. Hall, J. Barker, Y. Kaufman, A. Strahler, A. Huete, J.-P. Muller, V. Vanderbilt, Z. Wan, and P. Teillet, 1994: Terrestrial remote sensing science and algorithms planned for EOS/MODIS, Int. J. Remote Sens., vol. 15, no. 17, 3587-3620.

Sellers, P. J., F. G. Hall, G. Asrar, D. E. Strebel, and R. E. Murphy (1998). The first ISLSEP Field, Experiment (FIFE). Bull. *Amer. Meteorol. Soc.,* Vol. 69, no. 1, 22-27, 1988.

Vidal, R. C. and B. L. Blad, 1991: Atmospheric and emissivity correction of land surface temperature measured from satellite using ground measurements or satellite data, Int. J. Remote Sens., vol. 12, no. 12, 2449-2460.

Wan, Z., and J. Dozier (1996). A generalized split-window algorithm for retrieving land-surface temperature from space. *IEEE Trans. Geosci. Remote Sens*., 34, 892-905.

Wan, Z., and W. Snyder (1996). MODIS Land-Surface temperature algorithm theoretical basis document. MODIS ATBD

Watson, K. (1992). Two temperature method for measuring emissivity. *Remote Sens. Environ*, 42, 117-121.

Weng, F., and N. Grody (1998), Physical Retrieval of land surface temperature using the special sensor microwave imager. *J. Geophys. Res*., 103: 8839-8848.

Yu, Y. D. , A. Rothrock, and R. W. Lindsay, 1995: Accuracy of sea ice temperature derived from the advanced very high resolution radiometer, *J. Geophys. Res*., vol. 100, no. C3, 4525-4532.

Zhang, L., Lemeur, and J. P. Goutorbe, 1995: A one-layer resistance model for estimating regional evapotranpiration using remote sensing data, in Agricul. and Forest Meteorol., vol. 77, 241-261.